Steel and Composite Structures, *Vol. 56, No. 6 (2025) 487-497*
https://doi.org/10.12989/scs.2025.56.6.487

Monitoring for sinkholes using WT-SBAS-InSAR Analysis

Naeryoung Choi[1a], Lang Fu[2b], Jong-Sub Lee[3c] and Hyungjoon Seo*[1]

[1]*Department of Civil Engineering, Seoul National University of Science and Technology, SEOUL, 01811, Korea*
[2]*Department of Civil and Environmental Engineering, University of Liverpool, UK L69 7ZX, UK*
[3]*School of Civil, Environmental and Architectural Engineering, Korea University, 145, Anam-ro, Seongbuk-gu, Seoul 02841, Korea*

(Received May 22, 2025, Revised June 9, 2025, Accepted June 20, 2025)

Abstract. Sinkhole events are becoming more frequent in urban areas, making reliable ground monitoring essential. Ground displacement patterns around four sinkhole sites in Seoul were examined using Sentinel-1 SAR (Synthetic Aperture Radar) data collected from 2018 to 2025. The SBAS-InSAR (Small Baseline Subset Interferometric Synthetic Aperture Radar) technique was used to detect long-term subsidence trends. At each site, displacement data were compared between points close to the sinkholes and points farther away. To improve the detection of unusual surface changes, a method combining WT (Wavelet Transform) and SBAS-InSAR was developed, referred to as WT-SBAS-InSAR. Wavelet transform was applied to the original InSAR time series to identify localized frequency changes. These changes appeared near the time of known sinkhole events. InSAR data from distant control points did not show similar frequency increases. The results suggest that satellite-based interferometric methods, especially when combined with time-frequency analysis such as wavelet transform, can help detect early signs of sinkhole formation. These findings also indicate potential for future use in predictive modeling to improve urban infrastructure safety.

Keywords: complex networks; mathematical simulation; mechanical behavior; nanotechnology

1. Introduction

Sinkholes are a typical feature of karstic landscapes, where holes or collapsed structures are often formed when there is a rupture of the underlying rock or soil, while ground settlement is manifested when there is no sudden rupture during the slow subsidence and settlement process of the ground surface (Dobecki and Upchurch 2006, Waltham *et al*. 2005, Ford and Williams 2007, Abdi 2024). Sinkholes pose a major hazard to urban and suburban settlements, with serious consequences including destruction of infrastructure, ground settlement and the triggering of secondary hazards, especially in karstic development areas (Gutiérrez *et al*. 2014, Joyce *et al*. 2009). In the United States, damage from sinkhole collapses is estimated to exceed $300 million each year (Weary 2015). The formation of urban sinkholes is often closely linked to leaky water supply networks and inefficient stormwater management systems, both of which lead to an increase in subsurface seepage, thereby accelerating subsurface erosion and sinkhole development processes (Kaufmann and Quinif 2002, Van Den Eeckhaut *et al*. 2007). In addition, natural or anthropogenic vibrations, changes in surface loading, water intrusion or dewatering processes may trigger rapid sinkhole formation (Gutiérrez *et al*. 2014). Although sinkholes are often thought to lack obvious precursors, the presence of tensile cracks, pit wall cracks, and surface settlement can often serve as early warning signs that a sinkhole is imminent (Theron *et al*. 2017, Trollip 2006). Monitoring Sinkholes is a challenging task, as sinkhole formation processes are often hidden and sudden, with weak pre-settlement signals. Techniques such as GPR (Ground Penetrating Radar), ERT (Electrical Resistivity Tomography) and shallow seismic surveys are commonly used to monitor Sinkholes activities (Theron and Engelbrecht 2018, Carbonel *et al*. 2014). However, these techniques are costly, time-consuming and labor-intensive, and some are used only after ground deformation or structural damage has been observed (Engelbrecht *et al*. 2011, Engelbrecht and Inggs 2013). The formation process of Sinkholes may be accompanied by precursory surface settlement, signaling a potential risk of collapse. Therefore, early identification of precursor deformation patterns is important for early warning and monitoring of sinkhole hazards. LiDAR (Light Detection and Ranging) technology, such as laser scanning, has been applied to detect the deformation (Becker *et al*. 2024, Alseid *et al*. 2024, Zhao *et al*. 2022, Seo *et al*. 2022, Abbasi 2024). Recently, the radar remote sensing techniques, such as SAR (Synthetic Aperture Radar), provide a viable means of realizing surface deformation monitoring at relatively low cost (Love 1985, Crippen *et al*. 2016, Krieger *et al*. 2013, Yao *et al*. 2024). SAR imagery has broad spatial coverage and high spatial and temporal resolution, such as the Sentinel-1 satellite, which provides freely accessible data resources, making large-scale, continuous monitoring possible (Torres *et al*. 2012). In the past 3 decades, time-series InSAR (Interferometric Synthetic Aperture Radar) technology has

*Corresponding author, Ph.D. Associate Professor
E-mail: hjseo@seoultech.ac.kr
[a]Undergraduate Student
[b]Ph.D. Student
[c]Professor

ISSN: 1229-9367 (Print), 1598-6233 (Online)

been widely used in the field of surface settlement monitoring, such as SBAS-InSAR and PS-InSAR, which can realize millimeter-scale deformation measurements over long time spans, significantly improving the monitoring capability and spatial-temporal resolution of surface settlement (Yaseen *et al*. 2013, Sun *et al*. 2023, Wang *et al*. 2023b, Sowter *et al*. 2016, Hussain *et al*. 2022, Ramirez *et al*. 2022, Nur *et al*. 2024, Park *et al*. 2024). However, some of the sinkhole collapse events did not exhibit significant precursor settlement characteristics prior to their occurrence, and not all of the observed surface deformation processes eventually led to actual collapses (Calligaris *et al*. 2023). Some studies have successfully detected long-term precursor deformation or continuous settlement processes in major Sinkholes-prone areas using InSAR technology, which provides an important basis for early identification and risk assessment of sinkholes hazards (Chang and Hanssen 2014). InSAR technology has been widely used in monitoring research on the spatial and temporal evolution of Sinkholes in many locations. For example, it has been successfully used to monitor Sinkholes activities in the Dead Sea in Israel, the Bayou Corne area in Louisiana, United States of America, New Mexico and the Ebro Valley in Spain (Closson *et al*. 2005, Nof *et al*. 2013, Avni *et al*. 2016, Jones and Blom 2014, Rucker *et al*. 2013, Gutiérrez *et al*. 2011). Paine *et al*. were the first to combine InSAR and gravity measurements in the West Texas region of the United States to systematically investigate the deformation characteristics of local sinkholes (Paine *et al*. 2012). Kim *et al*. used satellite-borne Sentinel-1SAR data to find that continued settlement still exists in the areas surrounding two major collapse sinkholes in Wink, Texas (Kim *et al*. 2016, Kim and Lu 2018).

However, the limitation of the spatial resolution of the on-board sensors somewhat restricts the effectiveness of the InSAR technique in the application of refined settlement identification and sinkhole precursor monitoring. The SBAS-InSAR technique can provide continuous time series of surface deformation, but the in-depth understanding of the settlement process still needs to rely on the time-frequency domain analysis method.

Wavelet analysis, as a common time-frequency localization tool with the ability to capture signal features in time and frequency, has been widely validated in the analysis of seismic signals, climate change and other non-stationary time series (Cabieces *et al*. 2020, Janicke *et al*. 2009, Wang *et al*. 2023, Cheng *et al*. 2021, Fu *et al*. 2024). In particular, the Continuous Wavelet Transform (CWT), which can reveal the local change characteristics of the signals on different time scales, provides strong support for identifying the periodic evolution or sudden anomalies in the settlement process. Based on this, a WT-SBAS-InSAR framework is proposed in this study, aiming to explore the evolution of surface settlement in the sinkhole formation area from the perspective of time-frequency features. Firstly, the SBAS-InSAR technique is used to obtain the time series of settlement in the study area; subsequently, the continuous wavelet transform is applied to the locations where sinkholes have occurred, and the multiscale decomposition and periodic feature extraction are performed on the settlement signals, so as to explore the potential patterns and precursor features during the evolution of sinkholes, and to provide theoretical basis and data support for the early identification and early warning of similar disasters.

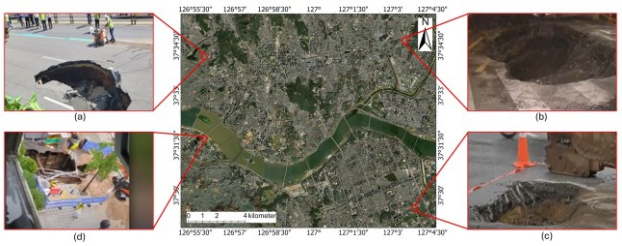

Fig. 1 Field photograph taken at time of sinkhole occurrence ((a) Site photo of Yeonhui-dong; (b) Site photo of Dongdaemun-gu; (c) Site photo of Gangnam-gu; (d) Site photo of Yeouido)

2. Study area and data collection

Sinkholes are phenomena in which the ground surface suddenly collapses due to the weakening or loss of the underlying support layer. They can occur not only under natural conditions but also as a result of human-induced factors such as underground excavation, leakage from aging buried pipelines, and excessive groundwater extraction. In urban areas, the unexpected occurrence of such sinkholes can lead to human casualties and disruption of urban infrastructure, emphasizing the need for precise preemptive monitoring and thorough investigation of underlying causes.

In this study, four locations in Seoul where sinkholes have previously occurred were selected to analyze ground behavior characteristics. (Fig. 1) The selected sites—Yeonhui-dong, Dongdaemun-gu, Gangnam-gu, and Yeouido—are representative urban areas characterized by complex subsurface structures, including subway tunnels, utility corridors, and underground malls, as well as a history of sinkhole incidents.

Yeonhui-dong is a densely built residential area in central Seoul where localized sinkholes have occurred near public roadways, highlighting the need to secure the stability of underground spaces. Dongdaemun-gu serves as a major transportation hub with multiple intersecting subway lines and large commercial facilities, resulting in a high density of subsurface infrastructure and raising concerns about long-term ground stability. Gangnam-gu, a district with a high concentration of high-rise buildings, underground parking facilities, and expansive underground malls, experienced a sinkhole in a commercial area with particularly intensive subsurface development. Yeouido, as Seoul's financial center, is densely packed with large office buildings and vital underground infrastructure; due to the area's economic importance, a sinkhole event could cause widespread disruption, underscoring the importance of proactive monitoring.

Due to the differences in geological settings,

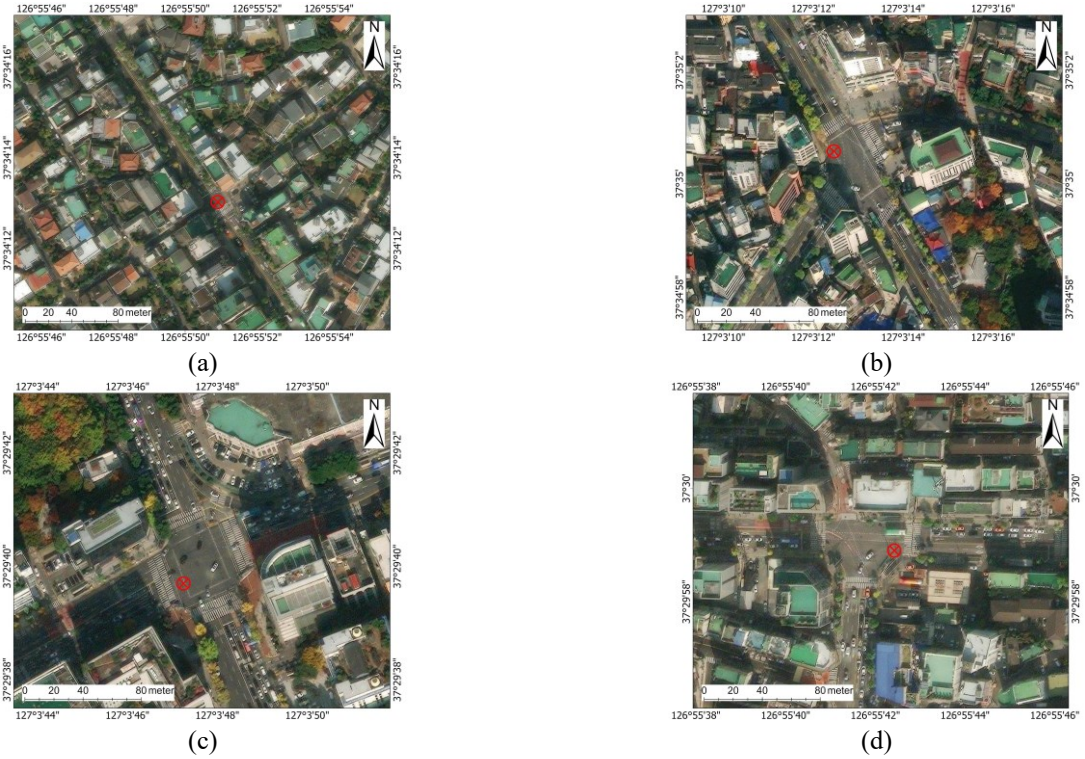

Fig. 2 Overview of sinkhole sites and observation points (a) Location of observation point in Yeonhui-dong; (b) Location of observation point in Dongdaemun-gu; (c) Location of observation point in Gangnam-gu; (d) Location of observation point in Yeouido)

underground infrastructure configurations, and patterns of urban development, these locations are well suited for a comparative evaluation of ground subsidence trends and potential precursor signals of sinkhole formation using satellite-based time series analysis.

To analyze ground displacement over time in areas prone to sinkholes, satellite images were used for location selection and visual inspection. Google Earth Pro was applied to identify four sites in Seoul where sinkholes had been reported in the past: Yeonhui-dong, Dongdaemun-gu, Gangnam-gu, and Yeouido (Fig. 2). At each site, six observation points were selected for further analysis.

Each site included three observation points located close to the sinkhole (about 5 to 20 meters away) and three points farther away (about 300 to 2,310 meters). This setup allowed comparison between areas affected by the sinkhole and nearby areas without visible damage. The location of each point was fixed based on clear features such as roads, buildings, and intersections in Google Earth. These reference points helped keep the alignment and time-series analysis of SAR data from InSAR consistent.

Setting observation points using satellite images was an important step before running the SBAS-InSAR analysis. This process gave a clear reference framework for comparing ground movement near sinkhole sites with areas farther away.

3. Methodology

To systematically analyze the surface deformation characteristics of the sinkhole formation area, this paper designs the overall research flow as shown in Figure 3. Firstly, SBAS-InSAR technology is used to monitor the surface settlement in the study area. The specific steps include image data preprocessing, connection map construction, main image selection, interferogram generation, phase map analysis and finally inversion to obtain a continuous surface deformation time series. On this basis, the CWT (Continuous Wavelet Transform) method is further applied to the locations where sinkhole settlements have occurred to characterize the time-frequency analysis of the surface deformation, to extract the periodic change pattern of the settlement process and its scale distribution characteristics, and to provide support for the understanding of the evolution mechanism of sinkholes.

3.1 SBAS-InSAR

In order to effectively deal with the spatio-temporal incoherence issue, this study adopts the SBAS-InSAR method, which divides the existing SAR image data into several subsets by setting reasonable temporal and spatial baseline thresholds, and ensures that the spatio-temporal baselines in each subset are smaller, thus improving the coherence (Berardino *et al*., 2002). The method not only fully utilizes the SAR data but also maintains a high observation accuracy while reducing the solution complexity.

If $N+1$ SAR images are acquired from t_0 to t_N, the images are divided into Z short baseline subsets for the spatio-temporal baseline constraints. In each subset, the

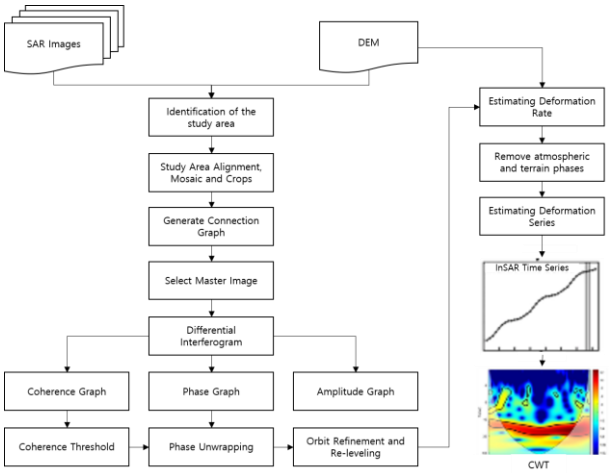

Fig. 3 Workflow

images are paired according to the short baseline criterion, and the interferograms are generated after differential interference processing. If N is specified to be an odd number, a total of M differential interferograms are generated from Z sets of images, and M can be expressed as:

$$\frac{N+1}{2} \le M \le N \times \frac{N+1}{2} \tag{1}$$

where N is the number of SAR images and M is the number of differential interferograms.

Taking t_0 as the initial moment, the cumulative shape variable $d(t_i,x,r)\ t \in (i=1,\dots\dots,N)$ of a certain image element (x,r) in the line-of-sight direction at t with respect to the moment of to is the quantity to be solved. If 2 SAR images at t_b and t_a (t_a is earlier than t_b) are paired to generate the kth differential interferogram, the resulting phase is $\eta\xi(t_k,x,r)\ k \in (i=1,\dots\dots,M)$. Neglecting the phase error due to noise such as atmospheric effects and elevation residuals, the phase at (x,r) is

$$\eta(t_k,x,r) = \eta\xi(t_b,x,r) - \eta\xi(t_a,x,r) = \frac{4\pi[d(t_b,x,r) - d(t_a,x,r)]}{\lambda} \tag{2}$$

where $\eta\xi(t_a,x,r)$ is the image phase at moment ; $\eta\xi(t_b,x,r)$is the image phase at moment ; $d(t_a,x,r)$is the line-of-sight oriented deformation at moment t_a ; $d(t_b,x,r)$ is the line-of-sight oriented deformation at moment t_b.

In actual processing, in addition to including the phase changes caused by the surface deformation, the error terms such as atmospheric delay, orbit error, elevation residuals and other noises are also inevitably superimposed. For this reason, the differential interferometric phase needs to be further modeled as an error and separated and corrected in the deformation extraction process. By establishing time-series observation equations for multiple short-baseline differential interferograms and employing inversion techniques such as the least-squares method, surface deformation information can be extracted on a continuous time series while suppressing the effect of errors.

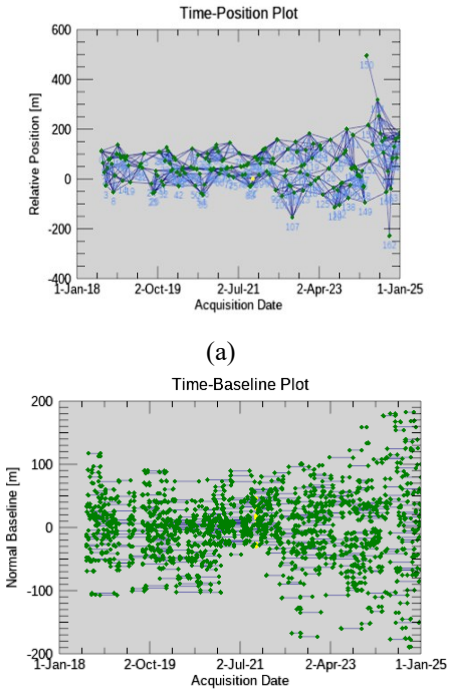

Fig. 4 Interferometric pair selection results for SBAS-InSAR analysis. ((a) Time–Position plot showing interferometric connections with no missing or disconnected scenes.; (b) Time–Baseline plot indicating all spatial baselines are within ±150 m.)

3.2 Continuous Wavelet Transform (CWT)

To reveal the local features and periodic variation rules of signals in different time scales, this paper adopts wavelet analysis for time-frequency feature extraction. As a commonly used time-frequency localization tool, wavelet analysis can provide high resolution in both time and frequency domains at the same time, which is suitable for dealing with multi-scale variation features in non-smooth signals. In this study, continuous wavelet transform (CWT) is chosen to decompose and analyze the time series data. The continuous wavelet transform of time series variables is defined as follows (Grinsted *et al*. 2004):

$$W_x(\zeta,S) = \int_{-\infty}^{+\infty} x(t)\varpi^*_{\zeta,S}(t)dt \tag{3}$$

where ϖ is the subwavelet, ϖ^* is the complex conjugate, ζ is the translation parameter, and S is the scaling factor.

By convolving the signal with wavelet functions with adjustable scale and translation parameters, CWT can reveal the local energy distribution characteristics of the signal at different scales while maintaining the temporal continuity, which provides a strong support for the subsequent analysis and prevention of sinkhole deformation. Morlet wavelets were used for continuous wavelet transformation in this study. The time series sampling interval was 12 days, based on the revisit period of Sentinel-1A. The frequency band of the transform was 0.0025 to 0.0625 cycles/day.

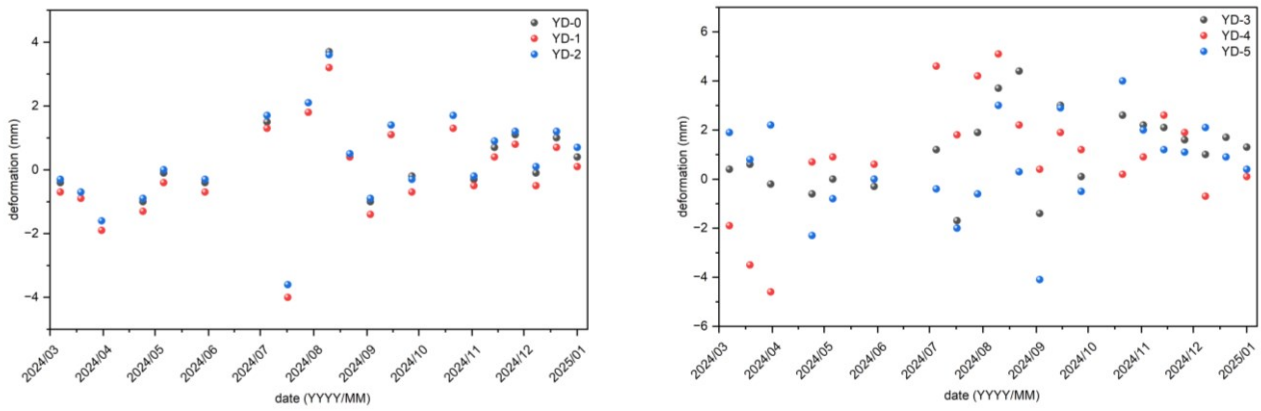

(a) (b)

Fig. 5 Ground deformation near (a) and distant from (b) Yeonhui-dong sinkhole site. ((a) Ground deformation graph near Yeonhui-dong sinkhole site; (b) Ground deformation graph at distant point from Yeonhui-dong sinkhole

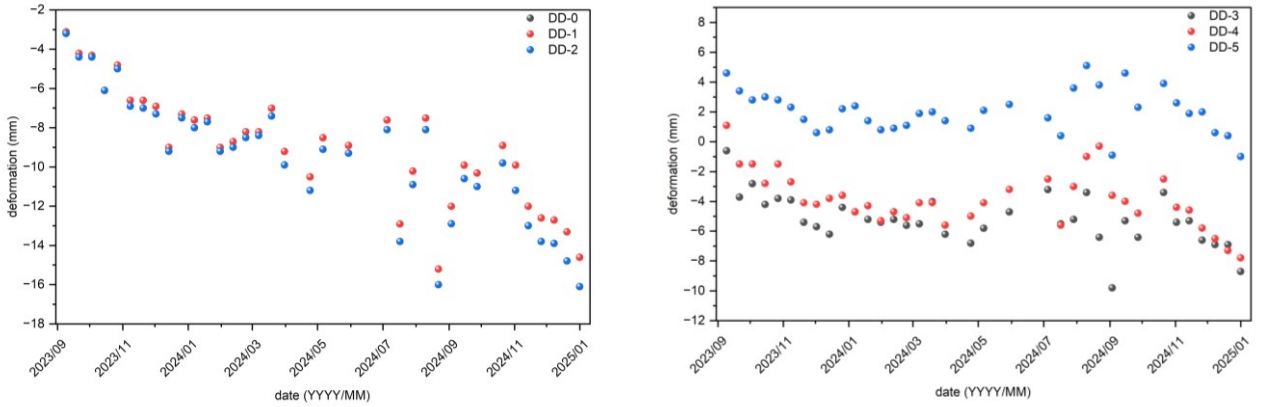

(a) (b)

Fig. 6 Ground deformation near (a) and distant from (b) Dongdaemun-gu sinkhole site. ((a) Ground deformation graph near Dongdaemun-gu sinkhole site; (b) Ground deformation graph at distant point from Dongdaemun-gu sinkhole

4. Results

A total of 140 Sentinel-1 images, taken at about 12-day intervals from 2018 to 2025, were used for processing. Interferometric pairs were created by linking only those images that met two baseline limits: a time gap of less than 180 days and a spatial distance within ±150 meters. This process formed a small baseline subset.

The stability of the network was checked using a time–spatial baseline plot (Time–Position Plot, Fig. 4(a)). The plot showed that all images were well connected under the set thresholds, with no missing or disconnected scenes. Each line in the plot represents one interferometric pair between a master image and a slave image. The time–baseline plot (Fig. 4(b)) also confirmed that the spatial baselines stayed within ±150 meters for all images. This result showed that the image pairs were consistent and of good quality throughout the study period.

Finally, cumulative ground subsidence was calculated for each observation point, serving as the foundational dataset for subsequent Wavelet Transform analysis and the identification of anomalous settlement behavior.

Fig. 5 analyzes ground displacement in the vicinity of the sinkhole that occurred in Yeonhui-dong. The time-series data span from early March 2024 to the start of 2025. At the sinkhole location (YD-0) and two adjacent points (YD-1, YD-2), located approximately 5 meters away, notable surface changes were observed prior to the event. The ground subsided by around 4.0 mm in mid-July and then rose by 3.7 mm in early August, just weeks before the sinkhole event on August 29. While these changes appear temporally close to the incident, it remains inconclusive whether they served as precursors. In contrast, the three distant points (YD-3 to YD-5), located up to 1.3 km away, displayed irregular displacement patterns with no temporal alignment to the event. This suggests that early warning signs, if any, may have been spatially limited to the immediate vicinity of the collapse.

In Fig. 6, ground movement patterns near the sinkhole in Dongdaemun-gu are examined using displacement data collected between September 2023 and January 2025. At the sinkhole point (DD-0) and its nearby sites (DD-1, DD-2), a consistent downward trend is evident throughout the observation period. Particularly, a sharp W-shaped deformation curve formed between early July and mid-September 2024, with a sudden drop of 16.0 mm recorded

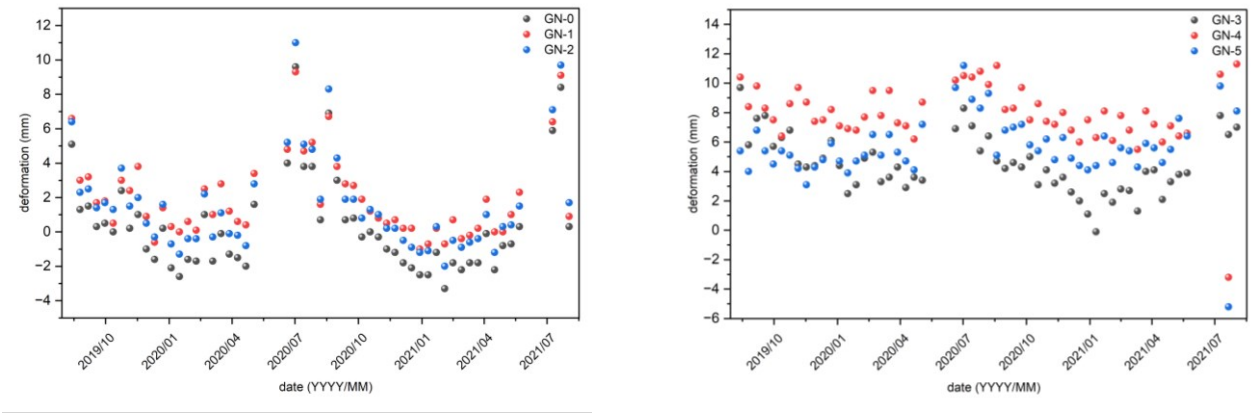

(a) (b)

Fig. 7 Ground deformation near (a) and distant from (b) Gangnam-gu sinkhole site. ((a) Ground deformation graph near Gangnam-gu sinkhole site; (b) Ground deformation graph at distant point from Gangnam-gu sinkhole)

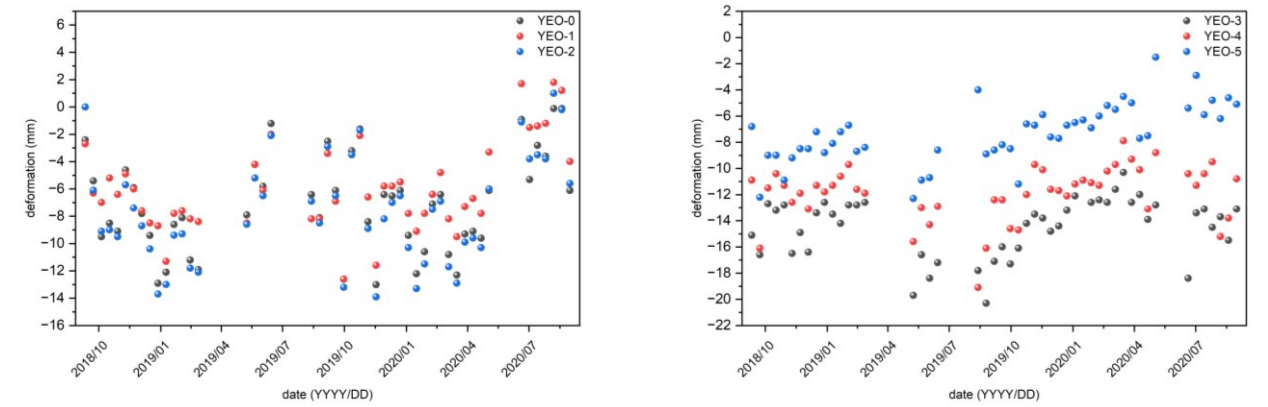

(a) (b)

Fig. 8 Ground deformation near (a) and distant from (b) Yeouido sinkhole site. ((a) Ground deformation graph near Yeouido sinkhole site; (b) Ground deformation graph at distant point from Yeouido sinkhole)

on August 22—just days before the sinkhole appeared on September 11. This distinct fluctuation may reflect ground instability that contributed to the event. Meanwhile, the more remote points (DD-3 to DD-5) showed smoother curves and gradual settlement patterns. Although some movement was detected near the time of collapse, its magnitude and rate were much lower, implying a reduced spatial impact away from the sinkhole center.

Fig. 7 presents subsidence patterns related to the Gangnam-gu sinkhole, using time-series data from mid-2019 to mid-2021. The sinkhole event, which occurred in August 2020, falls within a period of noticeable ground activity. At the main site (GN-0) and nearby points (GN-1, GN-2), significant uplift was observed in early July 2020, peaking at about 11 mm. A series of fluctuations followed, including a gradual decline, with minimum subsidence noted in early 2021. These dynamic changes, particularly between June and September 2020, align with the timing of the sinkhole and suggest potentially meaningful precursory behavior. On the other hand, the remote sites (GN-3 to GN-5) displayed similar displacement curves with no sharp deviations around the event. The changes there were milder and more gradual, indicating that ground instability was localized around the sinkhole site.

The analysis in Fig. 8 covers ground displacement leading up to the sinkhole in Yeouido, with data ranging from late 2018 to mid-2020. At the sinkhole location (YEO-0) and two surrounding points (YEO-1, YEO-2), continuous but modest fluctuations were observed. The largest settlement (13.9 mm) occurred in late 2019, months before the sinkhole, while no abrupt change was noted around the event on September 5, 2019. This indicates a relatively stable surface condition immediately preceding the incident. For the distant locations (YEO-3 to YEO-5), even larger settlements were recorded, with the maximum reaching 20.3 mm. However, these variations followed a gradual pattern and lacked any direct correlation with the sinkhole occurrence. Overall, while long-term trends were captured effectively, no short-term anomalies were distinct enough to indicate imminent collapse, underscoring the limitations of displacement-only analysis and motivating the introduction of Wavelet Transform in the next stage.

4.2 Wavelet transform data

Fig. 9 presents the results of time–frequency analysis

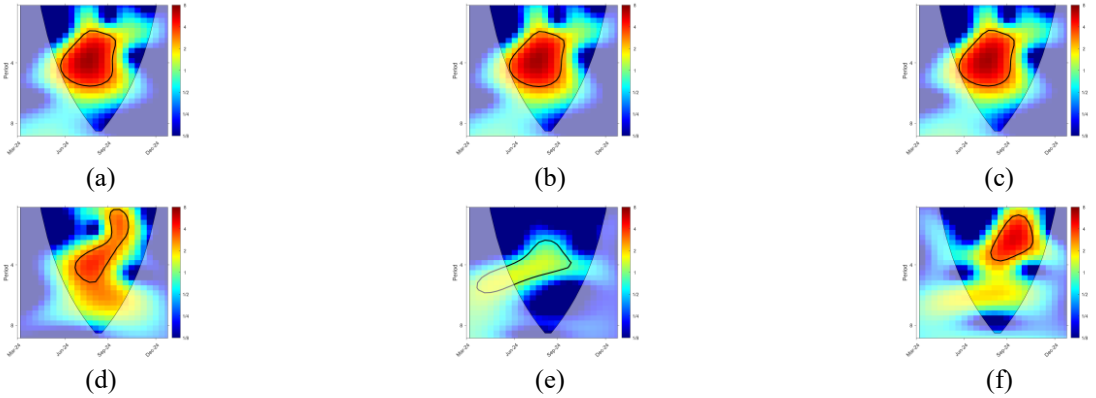

(a) (b) (c) (d) (e) (f)

Fig. 9 (a) Wavelet-based time–frequency spectrum at sinkhole location in Yeonhui-dong (YD-0); (b) Spectrum at nearby site 5 m from sinkhole (YD-1); (c) Spectrum at another nearby site 5 m from sinkhole (YD-2); (d) Spectrum at distant site 300 m from sinkhole (YD-3); (e) Spectrum at distant site 490 m from sinkhole (YD-4); (f) Spectrum at distant site 1,326 m from sinkhole (YD-5)

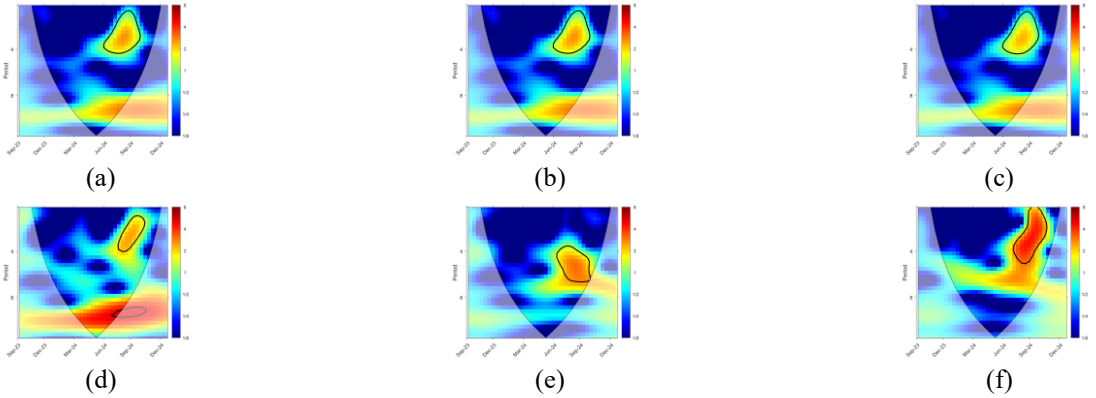

(a) (b) (c) (d) (e) (f)

Fig. 10 (a) Time-series ground deformation graph at sinkhole location in Dongdaemun-gu (DD-0); (b) Time-series ground deformation graph at nearby site 10 m from sinkhole (DD-1); (c) Time-series ground deformation graph at nearby site 20 m from sinkhole (DD-2); (d) Time-series ground deformation graph at nearby site 500 m from sinkhole (DD-3); (e) Time-series ground deformation graph at nearby site 748 m from sinkhole (DD-4); (f) Time-series ground deformation graph at nearby site 2,309 m from sinkhole (DD-5).

using the Wavelet Transform for the sinkhole event that occurred in Yeonhui-dong on August 29, 2024. The figure consists of six subplots, each visualizing the frequency spectrum of time-series ground displacement data collected at varying distances from the sinkhole.

Fig. 9(a) shows the spectrum for the sinkhole location (YD-0), while Figs. 9(b) and 9(c) correspond to two adjacent points (YD-1 and YD-2) located approximately 5 meters away. In all three upper plots, similar high-energy responses appear during a consistent time–frequency interval, with strong activity observed between July 5 and November 2, 2024. This period includes the sinkhole occurrence date and begins approximately two months prior. The black contours observed during this interval represent statistically significant signals, indicating that the energy concentration is not due to random noise but reflects a meaningful anomaly.

In contrast, Figs. 9(d), 9(e), and 9(f) display the spectral results for distant locations—YD-3, YD-4, and YD-5—located 300 m, 490 m, and 1,326 m from the sinkhole, respectively. These plots show markedly different patterns: the overall energy levels are low, and the black contours appear sporadically or are poorly defined. This suggests a weak or nonexistent correlation between ground displacement patterns at these locations and the timing of the sinkhole event.

These findings indicate that, in the vicinity of the sinkhole, statistically significant non-stationary signals emerged in a specific frequency band prior to the event—signals that were not detectable through cumulative displacement graphs alone. Conversely, the absence of such responses at greater distances underscores both the spatially localized nature of the ground disturbance and the limited range of the sinkhole's influence.

Fig. 10 shows the time-series ground movement related to the sinkhole event in Dongdaemun-gu. The data covers the period from September 9, 2023, to January 1, 2025. The sinkhole occurred on September 11, 2024, and was used as the reference point for analysis.

Fig. 10(a) shows the surface changes at the sinkhole point (DD-0) and at two nearby points (DD-1 and DD-2), located about 10 and 20 meters away. All three points

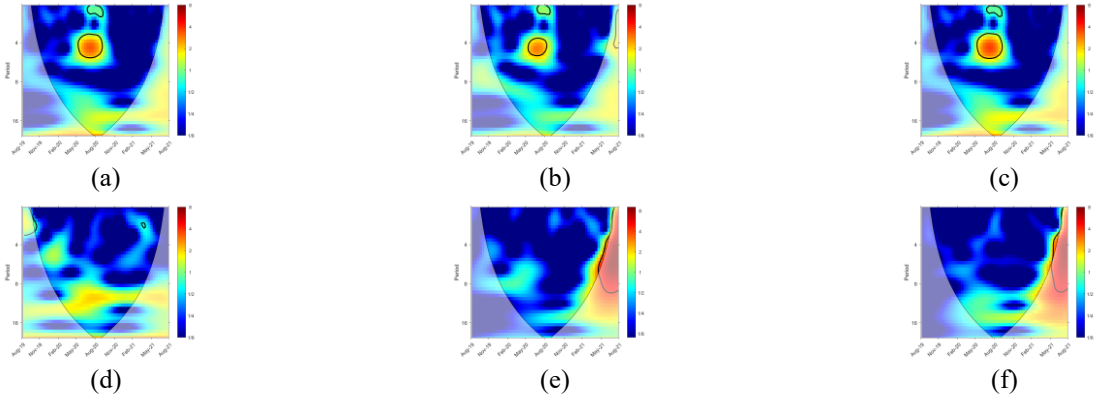

(a) (b) (c) (d) (e) (f)

Fig. 11 (a) Ground deformation graph at sinkhole location in Gangnam-gu (GN-0); (b) Ground deformation graph at nearby site 21 m from sinkhole (GN-1); (c) Ground deformation graph at nearby site 20 m from sinkhole (GN-2); (d) Ground deformation graph at distant site 1,720 m from sinkhole (GN-3); (e) Ground deformation graph at distant site 1,053 m from sinkhole (GN-4); (f) Ground deformation graph at distant site 1,100 m from sinkhole (GN-5).

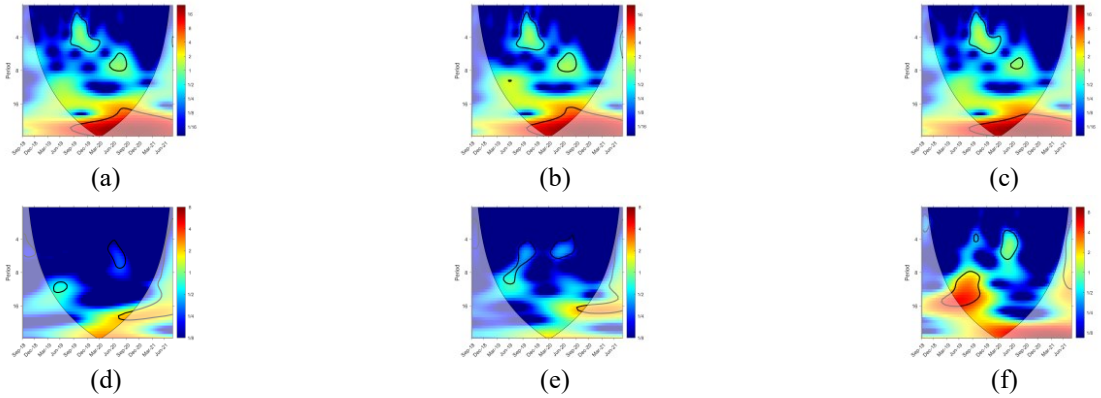

(a) (b) (c) (d) (e) (f)

Fig. 12 (a) Ground deformation graph at sinkhole location in Yeouido (YEO-0); (b) Ground deformation graph at nearby site 22 m from the sinkhole (YEO-1); (c) Ground deformation graph at nearby site 20 m from the sinkhole (YEO-2); (d) Ground deformation graph at distant site 495 m from sinkhole (YEO-3); (e) Ground deformation graph at distant site 500 m from sinkhole (YEO-4); (f) Ground deformation graph at distant site 997 m from sinkhole (YEO-5).

showed similar trends due to their close distance. The smallest recorded drop was 3.11 mm on September 9, 2023. The largest was 16.1 mm on January 1, 2025. A steady downward trend appeared over time, with sharp changes between July 5 and September 15, 2024. This section of the graph formed a W-shaped pattern. The biggest single drop, 16.0 mm, took place on August 22, 2024, just before the sinkhole event.

Fig. 11 presents the results of Wavelet Transform analysis applied to the sinkhole event that occurred in Gangnam-gu on August 3, 2020. Figs. 11(a), 11(b), and 11(c) (upper row) show the spectral results for the sinkhole location (GN-0) and two adjacent sites located 21 m (GN-1) and 20 m (GN-2) away, respectively. Figs. 11(d), 11€, and 11(f) (lower row) display the results for distant sites located 1,720 m (GN-3), 1,053 m (GN-4), and 1,100 m (GN-5) from the sinkhole.

At all three adjacent sites, a distinct high-energy response was observed from May 3 to October 6, 2020. Statistically significant anomalous signals appeared within similar time and frequency bands, enclosed by black contours. This interval begins approximately three months prior to the sinkhole event. The signal observed in Figure 11-a was particularly prominent, characterized by both high intensity and a wide area of influence, suggesting its potential as an early warning indicator.

In contrast, the distant sites exhibited generally weak frequency responses. Even where black contours were present, they appeared sporadically and lacked consistent timing or frequency structure. The power spectra at these

sites mostly displayed stable, low-energy distribution, typically represented in blue.

The Gangnam case demonstrates once again that Wavelet Transform analysis is effective for detecting early-stage, short-term ground anomalies. The early onset of anomalous signals and the consistent frequency response patterns across the sinkhole site and its adjacent areas highlight the method's utility in identifying precursory ground deformation.

Fig. 12 presents the results of Wavelet Transform analysis for the sinkhole event that occurred in Yeouido on September 5, 2019. Figs. 12(a), 12(b), and 12(c) (upper row) show the spectral data for the sinkhole location (YEO-0) and two adjacent sites located 22 m (YEO-1) and 20 m

(YEO-2) away, respectively. Figs. 12(d), 12(e), and 12(f) (lower row) correspond to distant locations situated 495 m (YEO-3), 500 m (YEO-4), and 997 m (YEO-5) from the sinkhole.

At the adjacent sites, the spectral patterns exhibit moderate but consistent responses, with several regions enclosed by black contour lines indicating elevated energy concentrations. While these responses are less pronounced than in previous cases, the spatial and temporal coherence across the three proximal points suggests the presence of potential precursory activity, albeit with lower intensity.

In contrast, the distant sites show relatively low energy levels throughout the observation period. The shape and extent of the contours are inconsistent, reducing the reliability of interpretation as clear indicators of anomaly. Specifically, Fig. 12(e) exhibits numerous scattered low-energy spots with almost no high-energy activity, while Figs. 12(d) and 12(f) show only sparse, small-scale contours without any evident spatial clustering.

These findings suggest that in the Yeouido case, the anomalous signals near the sinkhole site were weaker and less concentrated than in other cases, and no meaningful responses were observed at the more distant points. This further emphasizes the spatially localized nature of sinkhole-related ground disturbances and the need for high-resolution, site-specific monitoring strategies.

In this study, a time–frequency analysis incorporating the Wavelet Transform was conducted based on time-series ground displacement data derived from the SBAS-InSAR technique, with the aim of investigating its relationship to sinkhole occurrences. The results revealed that, at sites where sinkholes actually occurred, a noticeable increase in energy was observed within a specific high-frequency band (corresponding to periods of 4–8) several months prior to the event. These anomalies, which could not be identified through cumulative subsidence graphs alone, suggest the presence of early warning signals. In contrast, no similar frequency responses were detected at more distant sites within the same regions, confirming the localized nature of ground failure patterns.

These findings highlight the limitations of conventional time-domain monitoring approaches and underscore the added value of incorporating frequency-domain anomaly detection for more refined and proactive hazard prediction. The WT-SBAS-InSAR analytical framework proposed in this study offers a promising and reliable tool for future applications in urban ground stability monitoring, sinkhole risk forecasting, and the development of early warning systems.

5. Analysis

In this study, a WT-SBAS-InSAR Analysis utilizing Sentinel-1 SAR data was conducted for four sinkhole occurrence areas (Yonghi-dong, Dongdaemun-gu, Gangnam-gu, and Yeouido) in Seoul Metropolitan City. The analysis was designed to simultaneously consider time-series and cyclic characteristics of ground deformation in a framework that integrates SBAS-InSAR-based cumulative subsidence estimation and Wavelet Transform-based time-frequency analysis. For each region, ground behavior characteristics were analyzed by separating sinkhole-adjacent and comparison sites, thereby going beyond simple subsidence occurrence and quantitatively analyzing the presence and patterns of precursor phenomena.

First, the cumulative settlement data derived through the SBAS-InSAR technique showed a pattern of increasing displacement starting from the sinkhole occurrence point at sinkhole-adjacent points, but in most cases the trend was gradual or indistinct. In particular, in areas where the amount of subsidence was relatively small or progressed gradually, a limitation existed in that it was difficult to determine clear precursors based on the cumulative displacement graph alone.

Therefore, Wavelet Transform analysis, which was based on the same time series data, additionally captured signal characteristics in the time-frequency domain. As a result, near the point where the actual sinkhole occurred, a significant increase in energy in a specific frequency band (period 4-8 levels) was observed around the time of occurrence, which can be interpreted as a high-frequency response caused by structural heterogeneity and stress concentration in the ground. On the other hand, at the distant comparison sites within the same area, the energy distribution remained stable throughout the analysis period and no anomalous signals appeared.

This study shows that the deformation time series obtained by applying WT-SBAS-InSAR can identify long-term settlement trends and localized transient anomalies in areas prone to settlement. The ability to separate time-scale-specific energy concentrations enables the detection of subtle deformation features that may precede sudden surface collapse. These findings highlight the potential of wavelet-based analysis as a diagnostic tool for urban geohazard early warning systems and predictive models.

Although the method is promising, its extension to larger or denser urban areas faces many challenges. The computational demands of high-resolution time series analysis increase significantly with increasing spatial extent. In addition, spatial variability in surface conditions (vegetation, construction activities, or land use) can lead to reduced coherence and affect the stability of the time-frequency decomposition. Furthermore, current methods rely on manual interpretation of localized wavelet energy patterns; future research should aim to incorporate automated anomaly detection and classification algorithms to improve scalability and operational applicability. These limitations must be addressed to facilitate wider application of the technique in urban infrastructure monitoring frameworks.

6. Conclusions

WT-SBAS-InSAR Analysis was applied to four areas in Seoul where sinkholes had occurred: Yeonhui-dong, Dongdaemun-gu, Gangnam-gu, and Yeouido. The method used Sentinel-1 Synthetic Aperture Radar (SAR) data. This approach combined two parts: time-series analysis from the

Small Baseline Subset Interferometric SAR (SBAS-InSAR) and frequency-based analysis using wavelet transform. The goal was to track long-term subsidence and detect unusual short-term changes at the same time.

Cumulative ground movement graphs were created for each point. These graphs helped show the overall trend, especially for areas close to the sinkholes. In many cases, ground movement increased after the date when the sinkhole appeared. But when the amount of change was small or slow, these graphs made it hard to spot early signs before the sinkhole formed.

Wavelet transform was then used on the same time-series data. This helped track how the energy of the signal changed over time and across frequencies. At the locations where sinkholes appeared, a sharp rise in energy was found in a specific frequency band, around levels 4 to 8. This type of signal likely points to stress building up underground or uneven soil structure. At other nearby locations without sinkholes, the energy stayed stable and no clear unusual signals were found.

These results show that small but important changes before a sinkhole can be missed if only the total ground drop is considered. Wavelet-based analysis added extra value by picking up early signs that were otherwise hidden. The WT-SBAS-InSAR method showed that putting both approaches together gives a clearer picture of ground behavior. This makes it more useful for spotting warning signs before a sinkhole forms.

Cumulative graphs based on position alone are not enough to find local subsidence or early sinkhole risks in city areas. To find those, it is necessary to also look at repeating patterns and sudden changes in signal behavior. WT-SBAS-InSAR can be used in many areas such as checking ground stability in cities, building prediction tools for land risks, and setting up smart alert systems. This method provides a basic tool to help protect city infrastructure and reduce disasters.

Acknowledgments

This work was supported by the National Research Foundation of Korea (NRF) grant funded by the Korea government (MSIT) (No. RS-2021-NR060085).

References

Abbasi, M., Namadchi, A.H. and Abbasi, M. (2024), "Evaluation of machine learning algorithms in tunnel boring machine applications: A case study in Mashhad metro line 3", *Geo-Eng*., **15**, 28. https://doi.org/10.1186/s40703-024-00228-y.

Abdi, Y. (2024), "Investigation of the strength behavior and failure modes of layered sedimentary rocks under Brazilian test conditions", *Geo-Eng*., **15**, 6. https://doi.org/10.1186/s40703-024-00208-2.

Alseid, B., Chen, J., Huang, H. and Seo, H. (2024), "R-C-D-F machine learning method to measure for geological structures in 3D point cloud of rock tunnel face", *Tunnelling Underg. Space Technol*., **154**, 106071.

Avni, Y., Lensky, N., Dente, E., Shviro, M., Arav, R., Gavrieli, I., Yechieli, Y., Abelson, M., Lutzky, H. and Filin, S. (2016), "Self-accelerated development of salt karst during flash floods along the Dead Sea Coast, Israel", *J. Geophys. Res. Earth Surface*, **121**, 17-38.

Berardino, P., Fornaro, G., Lanari, R. and Sansosti, E. (2002), "A new algorithm for surface deformation monitoring based on small baseline differential SAR interferograms", *IEEE Transactions Geosci. Remote Sensing*, **40**, 2375-2383.

Cabieces, R., Krüger, F., Garcia-Yeguas, A., Villaseñor, A., Buforn, E., Pazos, A., Olivar-Castaño, A. and Barco, J. (2020), "Slowness vector estimation over large-aperture sparse arrays with the Continuous Wavelet Transform (CWT): Application to Ocean Bottom Seismometers", *Geophy. J. Int*., **223**, 1919-1934.

Calligaris, C., Forte, E., Busetti, A. and Zini, L. (2023), "A joint geophysical approach to tune an integrated sinkhole monitoring method in evaporitic environments", *Near Surface Geophy*., **21**, 317-332.

Carbonel, D., Rodríguez, V., Gutiérrez, F., McCalpin, J.P., Linares, R., Roqué, C., Zarroca, M., Guerrero, J. and Sasowsky, I. (2014), "Evaluation of trenching, ground penetrating radar (GPR) and electrical resistivity tomography (ERT) for sinkhole characterization", *Earth Surface Processes Landforms*, **39**, 214-227.

Chang, L. and Hanssen, R.F. (2014), "Detection of cavity migration and sinkhole risk using radar interferometric time series", *Remote Sensing Environ*., **147**, 56-64.

Closson, D., Karaki, N.A., Klinger, Y. and Hussein, M.J. (2005), "Subsidence and sinkhole hazard assessment in the southern Dead Sea area, Jordan", *Pure Appl. Geophys*., **162**, 221-248.

Crippen, R., Buckley, S., Agram, P., Belz, E., Gurrola, E., Hensley, S., Kobrick, M., Lavalle, M., Martin, J. and Neumann, M. (2016), "NASADEM global elevation model: Methods and progress", *Int. Archives Photogrammetry, Remote Sensing Spatial Information Sci*., **41**, 125-128.

Dobecki, T.L. and Upchurch, S.B. (2006), "Geophysical applications to detect sinkholes and ground subsidence", *Leading Edge*, **25**, 336-341.

Engelbrecht, J. and Inggs, M. (2013), "Recommendations for long-term operational DInSAR monitoring of mining-induced deformation in a dynamic agricultural region", *Proceedings of the 2013 IEEE International Geoscience and Remote Sensing Symposium (IGARSS)*, Melbourne, July.

Engelbrecht, J., Inggs, M.R. and Makusha, G. (2011), "Detection and monitoring of surface subsidence associated with mining activities in the Witbank Coalfields, South Africa, using differential radar interferometry", *South African J. Geology*, **114**, 77-94.

Ford, D. and Williams, P.D. (2007), *Karst Hydrogeology and Geomorphology*, John Wiley & Sons, Chichester, West Sussex, UK.

Grinsted, A., Moore, J.C. and Jevrejeva, S. (2004), "Application of the cross wavelet transform and wavelet coherence to geophysical time series", *Nonlinear Processes Geophys*., **11**, 561-566.

Gutiérrez, F., Galve, J.P., Lucha, P., Castañeda, C., Bonachea, J. and Guerrero, J. (2011), "Integrating geomorphological mapping, trenching, InSAR and GPR for the identification and characterization of sinkholes: A review and application in the mantled evaporite karst of the Ebro Valley (NE Spain)", *Geomorphology*, **134**, 144-156.

Gutiérrez, F., Parise, M., De Waele, J. and Jourde, H. (2014), "A review on natural and human-induced geohazards and impacts in karst", *Earth-Sci. Rev.*, **138**, 61-88.

Hussain, M.A., Chen, Z., Zheng, Y., Shoaib, M., Ma, J., Ahmad, I., Asghar, A. and Khan, J. (2022), "PS-InSAR based monitoring of land subsidence by groundwater extraction for Lahore Metropolitan City, Pakistan", *Remote Sensing*, **14**, 3950.

Janicke, H., Bottinger, M., Mikolajewicz, U. and Scheuermann, G.

(2009), "Visual exploration of climate variability changes using wavelet analysis", *IEEE Transactions Visualization Comput. Graphics*, **15**, 1375-1382.

Jones, C.E. and Blom, R.G. (2014), "Bayou Corne, Louisiana, sinkhole: Precursory deformation measured by radar interferometry", *Geology*, **42**, 111-114.

Joyce, K.E., Wright, K.C., Samsonov, S.V. and Ambrosia, V.G. (2009), "Remote sensing and the disaster management cycle", *Adv. Geosci. Remote Sensing*, **48**, 317-346.

Kaufmann, O. and Quinif, Y. (2002), "Geohazard map of cover-collapse sinkholes in the 'Tournaisis' area, southern Belgium", *Eng. Geology*, **65**, 117-124.

Kim, J.-W. and Lu, Z. (2018), "Association between localized geohazards in West Texas and human activities, recognized by Sentinel-1A/B satellite radar imagery", *Scientific Reports*, **8**, 4727.

Kim, J.-W., Lu, Z. and DeGrandpre, K. (2016), "Ongoing deformation of sinkholes in Wink, Texas, observed by time-series Sentinel-1A SAR interferometry (preliminary results)", *Remote Sensing*, **8**, 313.

Krieger, G., Zink, M., Bachmann, M., Bräutigam, B., Schulze, D., Martone, M., Rizzoli, P., Steinbrecher, U., Antony, J.W. and De Zan, F. (2013), "TanDEM-X: A radar interferometer with two formation-flying satellites", *Acta Astronautica*, **89**, 83-98.

Love, A. (1985), "In memory of Carl A. Wiley", *IEEE Antennas Propagation Soc. Newsletter*, **27**, 17-18.

Nof, R.N., Baer, G., Ziv, A., Raz, E., Atzori, S. and Salvi, S. (2013), "Sinkhole precursors along the Dead Sea, Israel, revealed by SAR interferometry", *Geology*, **41**, 1019-1022.

Paine, J.G., Buckley, S.M., Collins, E.W. and Wilson, C.R. (2012), "Assessing collapse risk in evaporite sinkhole-prone areas using microgravimetry and radar interferometry", *J. Environ. Eng. Geophys*., **17**, 75-87.

Ramirez, R.A., Lee, G.-J., Choi, S.-K., Kwon, T.-H., Kim, Y.-C., Ryu, H.-H., Kim, S., Bae, B. and Hyun, C. (2022), "Monitoring of construction-induced urban ground deformations using Sentinel-1 PS-InSAR: The case study of tunneling in Dangjin, Korea", *Int. J. Appl. Earth Observation Geoinform*., **108**, 102721.

Rucker, M.L., Panda, B.B., Meyers, R.A. and Lommler, J.C. (2013), "Using InSAR to detect subsidence at brine wells, sinkhole sites, and mines", *Carbonates Evaporites*, **28**, 141-147.

Sowter, A., Amat, M.B.C., Cigna, F., Marsh, S., Athab, A. and Alshammari, L. (2016), "Mexico City land subsidence in 2014–2015 with Sentinel-1 IW TOPS: Results using the Intermittent SBAS (ISBAS) technique", *Int. J. Appl. Earth Observation Geoinform.*, **52**, 230-242.

Sun, H., Peng, H., Zeng, M., Wang, S., Pan, Y., Pi, P., Xue, Z., Zhao, X., Zhang, A. and Liu, F. (2023), "Land subsidence in a coastal city based on SBAS-InSAR monitoring: A case study of Zhuhai, China", *Remote Sensing*, **15**, 2424.

Theron, A. and Engelbrecht, J. (2018), "The role of earth observation, with a focus on SAR interferometry, for sinkhole hazard assessment", *Remote Sensing*, **10**, 1506.

Theron, A., Engelbrecht, J., Kemp, J., Kleynhans, W. and Turnbull, T. (2017), "Detection of sinkhole precursors through SAR interferometry: Radar and geological considerations", *IEEE Geosci. Remote Sensing Lett*., **14**, 871-875.

Torres, R., Snoeij, P., Geudtner, D., Bibby, D., Davidson, M., Attema, E., Potin, P., Rommen, B., Floury, N. and Brown, M. (2012), "GMES Sentinel-1 mission", *Remote Sensing Environ*., **120**, 9-24.

Trollip, N.Y.-M.G. (2006), "The geology of an area south of Pretoria with specific reference to dolomite stability", Ph.D. Dissertation, University of Pretoria (South Africa), Pretoria.

Van den Eeckhaut, M., Poesen, J., Dusar, M., Martens, V. and Duchateau, P. (2007), "Sinkhole formation above underground limestone quarries: A case study in South Limburg (Belgium)", *Geomorphology*, **91**, 19-37.

Waltham, T., Bell, F.G. and Culshaw, M.G. (2005), *Sinkholes and Subsidence: Karst and Cavernous Rocks in Engineering and Construction*, Springer Science & Business Media, Dordrecht, Netherlands.

Wang, R., Ding, J., Ge, X., Wang, J., Qin, S., Tan, J., Han, L. and Zhang, Z. (2023a), "Impacts of climate change on the wetlands in the arid region of Northwestern China over the past 2 decades", *Ecological Indicators*, **149**, 110168.

Wang, R., Feng, Y., Tong, X., Li, P., Wang, J., Tang, P., Tang, X., Xi, M. and Zhou, Y. (2023b), "Large-scale surface deformation monitoring using SBAS-InSAR and intelligent prediction in typical cities of Yangtze River Delta", *Remote Sensing*, **15**, 4942.

Weary, D.J. (2015), "The cost of karst subsidence and sinkhole collapse in the United States compared with other natural hazards", *U.S. Geological Survey Open-File Report*, 2015-1017, Reston, VA, USA.

Yaseen, M., Hamm, N.A., Woldai, T., Tolpekin, V.A. and Stein, A. (2013), "Local interpolation of coseismic displacements measured by InSAR", Int. J. Appl. Earth Observation Geoinform., **23**, 1-17.